

**Sensitivity
simulations with dust
radiative forcing**

E. Bauer and
A. Ganopolski

Sensitivity simulations with direct radiative forcing by aeolian dust during glacial cycles

E. Bauer and A. Ganopolski

Potsdam Institute for Climate Impact Research, Potsdam, Germany

Received: 16 December 2013 – Accepted: 27 December 2013 – Published: 13 January 2014

Correspondence to: E. Bauer (eva.bauer@pik-potsdam.de)

Published by Copernicus Publications on behalf of the European Geosciences Union.

[Title Page](#)

[Abstract](#)

[Introduction](#)

[Conclusions](#)

[References](#)

[Tables](#)

[Figures](#)

[⏪](#)

[⏩](#)

[◀](#)

[▶](#)

[Back](#)

[Close](#)

[Full Screen / Esc](#)

[Printer-friendly Version](#)

[Interactive Discussion](#)



Sensitivity simulations with dust radiative forcing

E. Bauer and
A. Ganopolski

[Title Page](#)

[Abstract](#)

[Introduction](#)

[Conclusions](#)

[References](#)

[Tables](#)

[Figures](#)

[⏪](#)

[⏩](#)

[◀](#)

[▶](#)

[Back](#)

[Close](#)

[Full Screen / Esc](#)

[Printer-friendly Version](#)

[Interactive Discussion](#)

are larger in glacial than in interglacials by a factor of 2–2.5 in the equatorial Pacific (Anderson et al., 2006; Winckler et al., 2008) and by a factor of roughly 25 in Antarctica (Petit et al., 1999; Lambert et al., 2008). The paleo data on dust deposition thus suggest a larger atmospheric dust load in glacial than interglacial periods. Possible answers on how the associated dust radiative forcing could have differed between cooler and warmer climates, and which impact the dust radiative forcing might have had for the climate evolution can be studied by climate system models coupled with a dust cycle model. Currently, different dust cycle models which calculate dust emission fluxes, atmospheric transport and deposition rates are operational and show a wide divergence in the strength of the dust radiative forcing (Cakmur et al., 2006; Chin et al., 2002; Ginoux et al., 2006; Grini et al., 2005; Liao et al., 2004; Lunt and Valdes, 2002; Luo et al., 2003; Mahowald et al., 2006a; Miller et al., 2006; Myhre et al., 2003; Reddy et al., 2005; Takemura et al., 2009; Tanaka and Chiba, 2006; Tegen et al., 2002; Werner et al., 2002). Model simulations of the climate effect from the dust radiative forcing are still rare. A first study shows that the dust radiative forcing can produce a surface cooling of about -1 K for LGM conditions and of -0.4 K for preindustrial conditions (Mahowald et al., 2006b).

Important for calculations of the direct dust radiative forcing at TOA during glacial–interglacial climate cycles are reproductions of the atmospheric dust load and the surface albedo. A major cause for glacial–interglacial changes in dust load is presumably the changing dust emission from changes in vegetation distribution and sediment transport by glaciers. The use of the BIOME3 model which accounts for the carbon dioxide (CO_2) fertilization of vegetation (Haxeltine and Prentice, 1996) shows that the dust emission can grow from 8040 Tgyr^{-1} at preindustrial times to $10\,880 \text{ Tgyr}^{-1}$ at LGM which can increase further to $14\,020 \text{ Tgyr}^{-1}$ if also glaciogenic dust production is considered (Mahowald et al., 2006b). The larger glacial dust load is accompanied with larger surface albedo. Glacially increased ice and snow cover and reduced vegetation cover lead to an increased global mean surface albedo by about 30 % at LGM compared to present day. It will be demonstrated (Sect. 2.3) that the direct shortwave

**Sensitivity
simulations with dust
radiative forcing**E. Bauer and
A. Ganopolski[Title Page](#)[Abstract](#)[Introduction](#)[Conclusions](#)[References](#)[Tables](#)[Figures](#)[⏪](#)[⏩](#)[◀](#)[▶](#)[Back](#)[Close](#)[Full Screen / Esc](#)[Printer-friendly Version](#)[Interactive Discussion](#)

tropopause in all-sky conditions. The net forcing from the sum of shortwave and long-wave radiative forcing is given to be -0.02 W m^{-2} for LGM climate and -0.01 W m^{-2} for present climate, and the mean shortwave radiative forcing is -0.24 W m^{-2} for LGM and -0.10 W m^{-2} for present conditions. The dust radiative forcing presented by Claquin et al. (2003) and Takemura et al. (2009) span a wide range and intermediate values are presented by Mahowald et al. (2006b). The net dust radiative forcing at TOA for two LGM cases without and with glaciogenic dust sources is given to be -0.96 and -1.47 W m^{-2} , respectively, and for preindustrial conditions to be -0.87 W m^{-2} (Mahowald et al., 2006b).

Different possibilities might be responsible for the stronger negative dust radiative forcing obtained by Claquin et al. (2003) than by Takemura et al. (2009). The optical parameters used in the models are presumably similar and based on recent studies. Large differences are seen in the used dust loads implying differences in the interplay between dust load and surface albedo. The global dust load in Claquin et al. (2003) for present day is 35.3 Tg which is derived from the global dust emission flux of 3000 Tgyr^{-1} and the average lifetime of 4.3 days given in Mahowald et al. (1999). This load is by factor of 2.6 larger than the dust load of 13.6 Tg in Takemura et al. (2009). The latter small dust load results from a short dust lifetime of only 1.9 days although the simulated emission flux of 2594 Tgyr^{-1} (Takemura et al., 2009) corresponds to 86 % of the emission flux used by Claquin et al. (2003). Both studies use enhanced glacial dust emissions with compatible enhancement factors of 2.5 (Mahowald et al., 1999) and of 2.39 (Takemura et al., 2009) leading to also a larger glacial dust load in Claquin et al. (2003) than in Takemura et al. (2009). The stronger negative dust radiative forcing obtained by Claquin et al. (2003) could further result from a longer dust lifetime whereby dust aerosols are transported further downwind from source areas toward dark ocean areas. Hence, the larger dust load and the longer transport might explain the more negative forcing for LGM and present-day climates in Claquin et al. (2003) compared to the results in Takemura et al. (2009).

Sensitivity simulations with dust radiative forcing

E. Bauer and
A. Ganopolski

Title Page

Abstract

Introduction

Conclusions

References

Tables

Figures

⏪

⏩

◀

▶

Back

Close

Full Screen / Esc

Printer-friendly Version

Interactive Discussion

Dust radiative forcing depends further on micro-physical properties, as particle shape, mineralogy and mixing state among different aerosols. The size of the dust particles varies over orders of magnitude from less than 0.01 to more than 10 μm (Tegen and Lacis, 1996; Myhre and Stordal, 2001). This implies uncertainties in the calculation of radiative forcing because dust optical parameters are highly sensitive to particle size and radiation wavelength (Otto et al., 2009). The AEROCOM project provides values for effective optical parameters, as for the dust mass extinction efficiency and the complex refractive index. Of particular relevance for the present study is that the imaginary part of the refractive index for visible wavelengths (0.3–0.7 μm) is found to be by factor 2 to 6 smaller than considered earlier (Dubovik et al., 2002; Balkanski et al., 2007). An overestimation of the imaginary refractive index leads to an overestimation of the absorption of solar radiation and explains partly the diverse results on radiative forcing by mineral dust obtained by earlier studies (Overpeck et al., 1996; Tegen et al., 1996; Claquin et al., 1998). Recent estimates of the global mean shortwave forcing at TOA with a revised value of the imaginary refractive index for dust aerosols lie between -0.28 W m^{-2} (Reddy et al., 2005) and -0.68 W m^{-2} (Balkanski et al., 2007) for present-day in all-sky conditions. Another actual result is that the size distribution of atmospheric dust particles which are uplifted by convective events is found to be fairly constant and relatively insensitive to surface wind variations (Sow et al., 2009). According to this study, uplift events enrich primarily the number of particles smaller than 0.4 μm . Based on these measurements from dust storm events it can be assumed that dust aerosols transported over long distances have sizes mainly in the so called accumulation mode and it seems justified in the first place for the present study to limit on optical parameters typical for the accumulation mode.

Here, an Earth system model of intermediate complexity which includes atmosphere, ocean, vegetation, ice sheets and the dust cycle is used (Bauer and Ganopolski, 2010). In transient glacial–interglacial climate simulations the sensitivity of the direct shortwave radiative forcing (DRF) to changing parameters for dust optical properties and for the dust cycle model is studied. The dust DRF is tested by varying the crucial optical

Sensitivity simulations with dust radiative forcing

E. Bauer and
A. Ganopolski

[Title Page](#)[Abstract](#)[Introduction](#)[Conclusions](#)[References](#)[Tables](#)[Figures](#)[⏪](#)[⏩](#)[◀](#)[▶](#)[Back](#)[Close](#)[Full Screen / Esc](#)[Printer-friendly Version](#)[Interactive Discussion](#)

with a thermodynamic sea-ice model and the integration time step is five days. The vegetation model describes the vegetation cover on each land surface grid cell. The model distinguishes between the vegetation types grass and forest which are a function of growing-degree-days, precipitation and CO₂ fertilization (Brovkin et al., 2002). The desert area results from the remaining land surface fraction in a grid cell which is free of vegetation and ice cover. The shares of desert, vegetation and ice sheets on each land surface grid cell are computed on an annual time step. The size of each land surface cell is obtained from the land-sea mask. The ice-sheet model SICOPOLIS has a resolution of 1.5° in longitude and 0.75° in latitude. The three-dimensional polythermal ice model simulates the evolution of the ice-sheet elevation in the Northern Hemisphere with a half-year time step (Greve, 1997; Calov et al., 2005). The glacial–interglacial changes of the ice sheet distribution are fed back to calculations of the land–sea mask, the surface elevation, the freshwater flux and the surface albedo. The surface albedo is computed daily for each latitude–longitude grid cell taking account of the surface types land and ocean, snow properties, clear and cloudy conditions and the visible and infrared wavelength bands (Petoukhov et al., 2000).

The same climate model configuration as in Ganopolski et al. (2010) is used. The model is externally driven by the orbital-varying insolation (Berger, 1978) and the equivalent CO₂ concentration based on measurements of CO₂, CH₄ (methane) and N₂O (nitrous oxide) from Antarctica (Petit et al., 1999; Augustin et al., 2004). The dust deposition on snow surfaces is prescribed by adopting dust deposition fields for LGM and present day from Mahowald et al. (1999) as described in Calov et al. (2005). At the same time, unlike in our previous studies, the dust DRF is now simulated interactively. Figure 1a shows the radiative energy fluxes from the sun and from the greenhouse gases in terms of global and annual mean radiative forcing relative to preindustrial time (0 kyrBP = 0 ka) for the past 420 kyr. The mean solar radiative forcing is calculated with solar constant of 1360 W m⁻² and a mean planetary albedo of 0.3. The calculation of the mean longwave forcing by greenhouse gases is described in Ganopolski et al. (2010). The mean radiative forcing of the sun due to changes in Earth's orbital

Sensitivity simulations with dust radiative forcing

E. Bauer and
A. Ganopolski

Title Page

Abstract

Introduction

Conclusions

References

Tables

Figures

⏪

⏩

◀

▶

Back

Close

Full Screen / Esc

Printer-friendly Version

Interactive Discussion

parameters varies only by up to 0.3 W m^{-2} with the periods of eccentricity of about 100 and 400 kyr wherein short-term fluctuations of solar activity are neglected. Nevertheless, insolation changes are the major driver of the glacial–interglacial climate changes because the seasonal and latitudinal distribution of the insolation varies strongly on orbital time scales. This is usually shown by the maximum insolation at 65° N (so called Milankovitch forcing) which varies by more than 100 W m^{-2} on orbital time scales, while the greenhouse gas forcing varies more homogeneously with latitude and season by up to 3 W m^{-2} .

2.2 Description of dust cycle model

The emission, transport and deposition of atmospheric dust is computed with the dust cycle model (Bauer and Ganopolski, 2010) incorporated into the climate model (Sect. 2.1). The long-term changes in the dust distribution result from changes in the potential source areas. The source areas of terrestrial dust are described by three contributions which are firstly, the desert areas, secondly, the semi-arid areas with sparse grass cover and thirdly, the shelf areas exposed after ice sheet growth from sea-level decrease. The atmospheric dust distribution changes further with seasonal and regional variations in the wind fields, the snow cover and the hydrological cycle. The dust emission flux grows with the third power of the surface wind speed for speeds exceeding a threshold wind speed which is a function of soil dryness. The uplift of dust into the atmosphere is connected with the static stability of the atmosphere (Bauer and Ganopolski, 2010). Climate simulations with the one-way coupling between the climate model and the dust cycle model are called henceforth *off-line* simulations. Climate simulations in which the calculated dust DRF is fed back to the simulation are called *online* simulations including the climate response to dust DRF.

The adjustment of scaling parameters in the dust cycle model (Bauer and Ganopolski, 2010) is performed by off-line simulations. The main constraint is the reproduction of dust deposition fluxes in reasonable agreement simultaneously to the proxy

the following, the median ME value is used for reasons of simplicity and because possible variations of the dust ME associated with different types of dust sources are poorly known.

The imaginary part of the refractive index (RI) for dust aerosols is extremely variable and hard to constrain. Based on measurements of the Saharan Mineral Dust Experiment (SAMUM) over Morocco, the size-resolved refractive index for dust aerosols is found to have values for RI between 0.0008 and 0.0060 at 0.55 μm wavelength (Otto et al., 2009). Aircraft measurements during the Saharan Dust Experiment (SHADE) suggest RI = 0.0015 to be appropriate at 0.55 μm wavelength (Haywood et al., 2003). During the Dust and Biomass Burning Experiment (DABEX) over North Africa a rather small value of RI = 0.0004 is obtained from aircraft measurements for dust aerosols in the accumulation mode at 0.55 μm (Osborne et al., 2008). The AEROCOM project provides an effective value of RI = 0.0015 at mid-visible wavelength of 0.55 μm (Kinne et al., 2006). These investigations suggest an uncertainty range for dust RI from 0.0005 to 0.0060, and in the following transient simulations the dust radiative effects are studied for this range. It should be emphasized that the shortwave DRF is most effective in clear sky conditions and diminishes with growing cloudiness. Indirect effects from interactions between dust aerosols and clouds and longwave effects are not considered in the present study.

The theoretical studies by Liao and Seinfeld (1998) showed that the DRF at TOA induced by mineral dust aerosols can be divided into three regimes, a regime with negative forcing occurring over dark ocean surfaces, a regime with positive forcing occurring over bright snow and ice surfaces and a transition regime in which the sign of the radiative forcing changes. The larger the particle number concentration per volume of air and the lower the surface albedo are, the larger is the backscatter of the insolation at TOA. Else, the larger the particle number concentration and the larger the surface albedo are, the more visible light is absorbed owing to multiple reflections between the aerosols and the surface whereby the dust DRF at TOA can achieve positive values. The DRF at TOA changes its sign at the critical surface albedo which varies with dust

Sensitivity simulations with dust radiative forcing

E. Bauer and
A. Ganopolski

[Title Page](#)[Abstract](#)[Introduction](#)[Conclusions](#)[References](#)[Tables](#)[Figures](#)[⏪](#)[⏩](#)[◀](#)[▶](#)[Back](#)[Close](#)[Full Screen / Esc](#)[Printer-friendly Version](#)[Interactive Discussion](#)

Sensitivity simulations with dust radiative forcing

E. Bauer and
A. Ganopolski

Title Page

Abstract

Introduction

Conclusions

References

Tables

Figures



Back

Close

Full Screen / Esc

Printer-friendly Version

Interactive Discussion



AOT, the imaginary part of the refractive index and cloudiness. A consequence of the absorption and scattering effects by dust aerosols is that the shortwave radiative forcing at the surface is always negative and gets increasingly negative with increasing extinction of the insolation (Liao and Seinfeld, 1998). The reduction of insolation at the surface is connected with a gain of radiative energy in the atmosphere. The calculations of Liao and Seinfeld (1998) of the diurnal dust DRF at TOA and at the surface for cloud-free and cloudy conditions with a one-dimensional radiative transfer model based on Mie's theory for spherical particles are used for evaluating the shortwave scheme of the climate model.

The global and annual mean DRF calculated with the shortwave scheme (Petoukhov et al., 2000) is shown in Fig. 3a as a function of surface albedo for an atmospheric dust load of 100 mg m^{-2} as used by Liao and Seinfeld (1998). The shortwave scheme uses the two-stream delta-Eddington approximation (Shettle and Weinman, 1970) for wavelengths in the UV band ($0.2\text{--}0.4 \mu\text{m}$) and the visible band ($0.4\text{--}0.75 \mu\text{m}$) and includes molecular Rayleigh scattering, absorption by water vapor and carbon dioxide and the effects of cloudiness. The real part of the refractive index for aerosols is 1.5 in agreement with data (Otto et al., 2009). The dust DRF at TOA and at the surface are shown for cloud-free conditions and for a typical mean cloud fraction of 0.6. The sensitivity of the dust DRF with respect to particle absorption is shown by shaded areas using $\text{RI} = 0.001$ and $\text{RI} = 0.006$ as lower and upper absorption efficiencies, respectively. The boundaries of the shaded areas obtained with $\text{RI} = 0.006$ are directly comparable with the calculations of Liao and Seinfeld (1998). The simulated DRF at TOA and at the surface agree closely with their results for clear sky. For cloudy sky, the simulated TOA and surface DRF vary over a slightly larger range than seen in Liao and Seinfeld (1998) which is presumably due to the lower cloud fraction used in the present simulations.

The calculation of DRF at TOA for a dust load of 100 mg m^{-2} and $\text{RI} = 0.006$ shows that the critical surface albedo is close to the typical surface albedo for Sahara desert of $0.3\text{--}0.35$ in clear and cloudy conditions (Fig. 3a). The critical surface albedo increases to about 0.6 in clear and cloudy conditions for $\text{RI} = 0.001$ and in these circumstances

Sensitivity simulations with dust radiative forcing

E. Bauer and
A. Ganopolski

[Title Page](#)[Abstract](#)[Introduction](#)[Conclusions](#)[References](#)[Tables](#)[Figures](#)[⏪](#)[⏩](#)[◀](#)[▶](#)[Back](#)[Close](#)[Full Screen / Esc](#)[Printer-friendly Version](#)[Interactive Discussion](#)

the dust DRF is negative over the Sahara desert. However, the dust load over the Sahara desert and elsewhere during glacial periods often exceeds 100 mg m^{-2} and Fig. 3b shows the dust DRF for a dust load of 1000 mg m^{-2} analogously to Fig. 3a. The DRF is seen to increase by a factor of 8 to 10 for the ten-fold increase of the dust load and the critical surface albedo shifts to smaller values with increasing dust load. This means that a dust load of 1000 mg m^{-2} over a cloudless Sahara desert can produce a positive TOA forcing between 5 and 8 W m^{-2} for $\text{RI} = 0.006$ while for $\text{RI} = 0.001$ the TOA forcing can be negative between -11 and -9 W m^{-2} . Hence Fig. 3b suggests that even if a high dust load occurs over a bright desert area the dust DRF at TOA can be small if RI lies between 0.001 and 0.006. At the surface, the direct radiative forcing is negative for all values of dust load and surface albedo. The surface DRF gets increasingly negative with increasing extinction of the insolation in the atmosphere (Fig. 3).

The actual dust DRF is hard to constrain unless consistent model simulations and observational data are available. The provision of data on dust radiative forcing is hindered by the interactions among aerosols, radiation and cloudiness. Available satellite-based estimates on dust DRF can give support to simulated dust DRF in clear-sky conditions. Measurements of shortwave radiative forcing at TOA in clear-sky conditions over the Atlantic Ocean between 0 and 30° N can be ascribed to the abundant dust aerosols for which the forcing is estimated to be $-7.75 \pm 0.86 \text{ W m}^{-2}$ (Christopher and Jones, 2007). This estimate is obtained for dust AOT at the wavelength of $0.55 \mu\text{m}$ during the months June to August in the years 2000 to 2005. The longwave dust radiative forcing is positive and is found to cancel nearly 20% of the negative shortwave forcing, thus the net radiative forcing is given to be $-6.31 \pm 1.16 \text{ W m}^{-2}$ (Christopher and Jones, 2007). The mean direct radiative effect at TOA for one year (2000–2001) over global land areas in clear-sky conditions is estimated to be $-5.1 \pm 1.15 \text{ W m}^{-2}$ (Patadia et al., 2008). This estimate is obtained for AOT at wavelength of $0.558 \mu\text{m}$ including contributions from different natural and anthropogenic aerosols but excluding aerosol loads over regions with high surface reflectance. A detailed analysis for the Sahara

Sensitivity simulations with dust radiative forcing

E. Bauer and
A. Ganopolski

Title Page

Abstract

Introduction

Conclusions

References

Tables

Figures

⏪

⏩

◀

▶

Back

Close

Full Screen / Esc

Printer-friendly Version

Interactive Discussion

with a surface albedo between 0.35 and 0.40 shows that the TOA shortwave flux is small and nearly insensitive to increasing AOT (Patadia et al., 2009; Yang et al., 2009). This low sensitivity derived from satellite observations is supported by four-stream radiative transfer calculations for clear-sky conditions. Hence in clear-sky conditions over the Sahara, the TOA shortwave radiative forcing can be negligible in comparison to the TOA longwave radiative forcing (Patadia et al., 2009) and the net direct radiative forcing could be positive.

3 Simulations of glacial cycles

In our previous study, the dust cycle model was tested in off-line simulations over the last four glacial cycles with the coupled model for the climate system and the ice sheets (Bauer and Ganopolski, 2010). Here the dust DRF is calculated with parameters varied within uncertainty ranges and results from online simulations with the dust DRF are discussed for the last 140 kyr. Theoretical considerations indicate that the DRF by dust aerosols depends crucially on two key factors. These are the atmospheric dust load and the absorption-scattering efficiency of dust aerosols which both include large uncertainties. Possible climatic effects are explored by six simulation experiments using an upper and a lower limit for dust load and for both loads three different absorption efficiencies. The upper and lower limits for dust load are obtained from solutions L1 and L2 of the dust cycle model (Sect. 2.2), and low, medium and upper absorption efficiencies are described by the imaginary refractive index RI of 0.0005, 0.0015 and 0.0060, respectively (Sect. 2.3).

3.1 Variations in dust DRF

The possible range of the annual and global mean dust AOT over the last 140 kyr obtained from solutions L1 and L2 is shown Fig. 4a. The dust AOT from solution L1 varies between about 0.02 and 0.10 and from solution L2 between about 0.015 and 0.060.

Sensitivity simulations with dust radiative forcing

E. Bauer and
A. Ganopolski

Title Page

Abstract

Introduction

Conclusions

References

Tables

Figures

⏪

⏩

◀

▶

Back

Close

Full Screen / Esc

Printer-friendly Version

Interactive Discussion

The dust AOT varies with the period of climatic precession in correspondence to the dust emission flux (Fig. 1b). The previous peak value in AOT occurs at the beginning of the LGM period which is defined from 23 to 19 ka (Waelbroeck et al., 2009). The previous minimum in AOT occurs in the early Holocene at 9 ka when a large fraction of the Sahara is simulated with grass cover. Peak values in dust AOT concur with enhanced surface albedo from increased snow and ice cover during cold periods (Fig. 4a). The simulated range of dust AOT for present-day (preindustrial) climate of 0.032–0.051 (Table 3) lies well in the interval 0.012–0.054 obtained from models participating in the AEROCOM exercise (Kinne et al., 2006).

The annual and global mean dust DRF at TOA from the six simulation experiments (Fig. 4b) vary with the period of climatic precession as dust AOT. The dust DRF calculated for each imaginary refractive index RI is displayed by a shaded band of which the boundaries result from solutions L1 and L2. The dust DRF obtained with RI of 0.0005 and 0.0015 is negative and correlated with dust AOT from both solutions L1 and L2. This is different when RI = 0.0060 is used. The dust DRF from L1 fluctuates around zero with positive values for large dust AOT, and the dust DRF from L2 is negative and anticorrelated with dust AOT. The strongest negative DRF of -0.92 W m^{-2} at 21 ka and -0.59 W m^{-2} at 0 ka is obtained in the experiment with low absorption efficiency and upper dust load (Table 3). At the surface, the dust radiative forcing is negative and its strength increases with dust AOT and absorption efficiency (Fig. 4c). The annual and global mean surface radiative forcing from the six experiments range from -0.95 to -2.4 W m^{-2} for LGM climate and from -0.6 to -1.35 W m^{-2} for present-day climate. These ranges of the surface radiative forcing enclose the values presented in Mahowald et al. (2006b) which are -1.28 and -1.59 W m^{-2} for two LGM cases and -1.03 W m^{-2} for the preindustrial case.

The annual zonal means of dust AOT show the largest values in the latitudes with the major dust sources. These are in the latitude band $20\text{--}30^\circ \text{ N}$ for both solutions and at both periods 21 and 0 ka (Fig. 5a and b). The dust DRF at TOA from the six sensitivity experiments in the northern subtropical latitudes is seen to be substantial and at the

**Sensitivity
simulations with dust
radiative forcing**E. Bauer and
A. Ganopolski[Title Page](#)[Abstract](#)[Introduction](#)[Conclusions](#)[References](#)[Tables](#)[Figures](#)[⏪](#)[⏩](#)[◀](#)[▶](#)[Back](#)[Close](#)[Full Screen / Esc](#)[Printer-friendly Version](#)[Interactive Discussion](#)

same time highly uncertain (Fig. 5c and d). In the latitude band of maximum dust load, the dust DRF is either negative or positive when using the low or upper absorption efficiency, respectively. This is most obvious for LGM conditions when the dust DRF from solution L1 changes from about -3 to $+2 \text{ W m}^{-2}$ with RI changing from 0.0005 to 0.0060 (Fig. 5c). The experiment with medium absorption efficiency leads to a negative DRF for both solutions and periods, however, the sensitivity of dust DRF on dust load in northern subtropical latitude band is reduced because the surface albedo of the Sahara is close to the critical value (Fig. 3). In consequence of the localized dust load, the dust DRF at the surface concentrates in northern subtropics (Fig. 5e and f). The larger the absorption of the insolation by dust load is the stronger is the decrease of solar radiation energy at the surface and the gain of radiative energy in the atmosphere above. For LGM conditions, the surface DRF in the subtropics increases from about -3.5 up to -9.3 W m^{-2} with RI increasing from 0.0005 to 0.0060.

The geographical irregular distribution of annual mean dust DRF at TOA is shown for solution L1 with medium absorption efficiency at LGM and present-day climates in Fig. 6. For LGM climate (Fig. 6a), the dust DRF in the grid cell east of the Sahara is stronger than -6 W m^{-2} , north and south of the Sahara stronger than -5 W m^{-2} , and over large areas of Asia between -2 and -3 W m^{-2} . In the northern low latitudes of the Atlantic and subtropical latitudes of south America and Australia the DRF is between -1 and -2 W m^{-2} . Over areas covered with snow or ice in high latitudes the dust DRF reaches small positive values. For present day climate (Fig. 6b), the dust DRF is negative and concentrated over north Africa and over Asia. The strongest negative forcing of about -4 W m^{-2} occurs over land surrounding the Sahara grid cell in which the maximum dust load occurs (Fig. 2a). The distributions of dust DRF (Fig.) 6 compare reasonable with the maps of net dust radiative forcing shown in Takemura et al. (2009) except for the positive forcing over the Sahara in Takemura et al. (2009). That positive forcing results presumably from the longwave forcing which can outbalance the negative shortwave forcing in the net forcing.

Sensitivity simulations with dust radiative forcing

E. Bauer and
A. Ganopolski

Title Page

Abstract

Introduction

Conclusions

References

Tables

Figures

⏪

⏩

◀

▶

Back

Close

Full Screen / Esc

Printer-friendly Version

Interactive Discussion

the emission flux increases by more than 900 Tgyr^{-1} with the low absorption efficiency and decreases by up to 800 Tgyr^{-1} with the high absorption efficiency. The reduced emission flux obtained with $\text{RI} = 0.0060$ results from shrinking desert areas in Africa and northward extending grass areas in Asia and a reduced uplift of dust into the atmosphere. In contrast the use of $\text{RI} = 0.0005$ leads to an increased dust emission flux because of growing desert areas, reduced grass cover and a lower sea level attributed to growing inland ice volume. The experiments conducted with $\text{RI} = 0.0015$ which give glacial–interglacial variations in the dust DRF from -0.7 to -0.2 Wm^{-2} (Fig. 4b) produce random anomalies in the dust emission fluxes with amplitudes up to 300 Tgyr^{-1} . Figure 7b also shows the dust emission flux from the off-line simulation and the induced upper and lower limits obtained from the online simulations with solution L1 and low and high absorption efficiencies, respectively. The maximum dust emission flux at LGM which is 3400 Tgyr^{-1} in the off-line simulation covers a wide range from 2400 to 3900 Tgyr^{-1} in the online simulations.

An independent measure to evaluate the output of the online simulations is the comparison of the simulated ice volume with sea level reconstructions (Waelbroeck et al., 2009) shown in Fig. 7c. The simulated ice volume is seen to respond to the dust DRF at TOA (Fig. 4b) with some time delay. The simulated sea level with the upper absorption efficiency matches the sea level of the off-line simulation and both simulations reproduce the reconstruction closely with a slight underestimation of the sea level drop at LGM. The sea level obtained with the medium absorption efficiency underestimates the sea level from the Eemian period onward and agrees closely with the reconstructions at LGM. Afterward the simulated sea level falls further until about 18 ka and reaches the Holocene value with delay by about 10 kyr. The simulations with the lower absorption efficiency produce strongly falling sea levels after 70 ka. Toward glacial maximum the sea level from solution L2 dropped to about -160 m and from solution L1 to about -210 m . Hence, the negative dust DRF obtained with $\text{RI} = 0.0005$ activates a positive feedback loop. The negative DRF grows through increasing dust emissions from cooler and dryer climate conditions implying a further lowering of the sea level in the

Sensitivity simulations with dust radiative forcing

E. Bauer and
A. Ganopolski

[Title Page](#)

[Abstract](#)

[Introduction](#)

[Conclusions](#)

[References](#)

[Tables](#)

[Figures](#)

[⏪](#)

[⏩](#)

[◀](#)

[▶](#)

[Back](#)

[Close](#)

[Full Screen / Esc](#)

[Printer-friendly Version](#)

[Interactive Discussion](#)

induced by dust aerosols could affect the glacial–interglacial climate evolution. The interplay between large-scale climate characteristics and micro-physical properties of dust aerosols is described in an efficient way to test the possible impact of the direct shortwave radiative forcing by dust aerosols on glacial cycle simulations.

The atmospheric distribution of dust and the absorption-scattering efficiency of dust aerosols are identified as key factors controlling the dust DRF. Constraints for the present-day atmospheric dust load and for the imaginary part of the refractive index RI are available from analyzes of various data and simulations with general circulation models. These constraints define a set of simulation experiments which account for upper and lower limits in dust load and RI. The resulting mean dust DRF span a wide uncertainty range. For LGM climate at 21 ka, the dust DRF at TOA ranges from -0.92 to $+0.04 \text{ W m}^{-2}$ and for present day climate from -0.59 to -0.06 W m^{-2} . Yet, these values are in the range obtained from time slice simulations with general circulation models (Claquin et al., 2003; Takemura et al., 2009).

The dust DRF simulated with the different parameter settings is applied for the first time in different simulations to study glacial cycles with the Earth system model of intermediate complexity CLIMBER-2. The main conclusions from the these simulation experiments are as follows. First, the dust DRF is highly localized showing annual mean values of several W m^{-2} in the regions close to major dust sources and negligible values elsewhere. Therefore, global means of dust DRF should be used with caution for estimating its global-scale impact on temperature. Second, the dust DRF is a nonlinear function of insolation, dust load, surface albedo, cloudiness and absorption-scattering efficiency leading to variable strength of the dust DRF and even the sign of the DRF is uncertain. This is an explanation for the wide uncertainty range of dust DRF. Third, the dust DRF induces changes in temperature and precipitation fields. This climate response is found strongly sensitive to dust distribution and to absorption efficiency because the dust cycle is part of a feedback loop. In simulations with upper dust load and low RI of 0.0005, the dust DRF is negative and the induced mean SAT cooling is 2.3 K at LGM and 1.1 K at present day compared to the off-line simulation. The

References

- Anderson, R., Fleisher, M., and Lao, Y.: Glacial–interglacial variability in the delivery of dust to the central equatorial Pacific Ocean, *Earth Planet. Sc. Lett.*, 242, 406–414, 2006. 152
- Archer, D., Winguth, A., Lea, D., and Mahowald, N.: What caused the glacial/interglacial atmospheric $p\text{CO}_2$ cycles?, *Rev. Geophys.*, 38, 159–189, 2000. 153
- Augustin, L., Barbante, C., Barnes, P. R. F., Barnola, J. M., Bigler, M., Castellano, E., Cattani, O., Chappellaz, J., Dahl-Jensen, D., Delmonte, B., Dreyfus, G., Durand, G., Falourd, S., Fischer, H., Flückiger, J., Hansson, M. E., Huybrechts, P., Jugie, G., Johnsen, S. J., Jouzel, J., Kaufmann, P., Kipfstuhl, J., Lambert, F., Lipenkov, V. Y., Littot, G. C., Longinelli, A., Lorrain, R., Maggi, V., Masson-Delmotte, V., Miller, H., Mulvaney, R., Oerlemans, J., Oerter, H., Orombelli, G., Parrenin, F., Peel, D. A., Petit, J.-R., Raynaud, D., Ritz, C., Ruth, U., Schwander, J., Siegenthaler, U., Souchez, R., Stauffer, B., Steffensen, J. P., Stenni, B., Stocker, T. F., Tabacco, I. E., Udisti, R., Van De Wal, R. S. W., Van Den Broeke, M., Weiss, J., Wilhelms, F., Winther, J.-G., Wolff, E. W., and Zucchelli, M.: Eight glacial cycles from an Antarctic ice core, *Nature*, 429, 623–628, 2004. 157, 159
- Balkanski, Y., Schulz, M., Claquin, T., and Guibert, S.: Reevaluation of Mineral aerosol radiative forcings suggests a better agreement with satellite and AERONET data, *Atmos. Chem. Phys.*, 7, 81–95, doi:10.5194/acp-7-81-2007, 2007. 155
- Bauer, E. and Ganopolski, A.: Aeolian dust modeling over the past four glacial cycles with CLIMBER-2, *Global Planet. Change*, 74, 49–60, 2010. 155, 156, 158, 160, 165
- Bauer, E., Ganopolski, A., and Montoya, M.: Simulation of the cold climate event 8200 yr ago by meltwater outburst from Lake Agassiz, *Paleoceanography*, 19, PA3014, doi:10.1029/2004PA001030 2004. 156
- Bauer, E., Petoukhov, V., Ganopolski, A., and Eliseev, A. V.: Climatic response to anthropogenic sulphate aerosols versus well-mixed greenhouse gases from 1850 to 2000 AD in CLIMBER-2, *Tellus B*, 60, 82–97, 2008. 156
- Berger, A. L.: Long-term variations of daily insolation and Quaternary climatic changes, *J. Atmos. Sci.*, 35, 2362–2367, 1978. 157
- Berger, A., Loutre, M.-F., and Tricot, C.: Insolation and Earth's orbital periods, *J. Geophys. Res.*, 98, 10341–10362, 1993. 159

CPD

10, 149–193, 2014

Sensitivity simulations with dust radiative forcing

E. Bauer and
A. Ganopolski

Title Page

Abstract

Introduction

Conclusions

References

Tables

Figures

⏪

⏩

◀

▶

Back

Close

Full Screen / Esc

Printer-friendly Version

Interactive Discussion

Sensitivity simulations with dust radiative forcing

E. Bauer and
A. Ganopolski

[Title Page](#)[Abstract](#)[Introduction](#)[Conclusions](#)[References](#)[Tables](#)[Figures](#)[Back](#)[Close](#)[Full Screen / Esc](#)[Printer-friendly Version](#)[Interactive Discussion](#)

- Bonelli, S., Charbit, S., Kageyama, M., Woillez, M.-N., Ramstein, G., Dumas, C., and Quiquet, A.: Investigating the evolution of major Northern Hemisphere ice sheets during the last glacial-interglacial cycle, *Clim. Past*, 5, 329–345, doi:10.5194/cp-5-329-2009, 2009. 156
- Bopp, L., Kohfeld, K. E., Le Quéré, C., and Aumont, O.: Dust impact on marine biota and atmospheric CO₂ during glacial periods, *Paleoceanography*, 18, 1046, doi:10.1029/2002PA000810, 2003. 153
- Brovkin, V., Bendtsen, J. R., Claussen, M., Ganopolski, A., Kubatzki, C., Petoukhov, V., and Andreev, A.: Carbon cycle, vegetation, and climate dynamics in the Holocene: experiments with the CLIMBER-2 model, *Global Biogeochem. Cy.*, 16, 1139, doi:10.1029/2001GB001662, 2002. 157
- Brovkin, V., Ganopolski, A., Archer, D., and Rahmstorf, S.: Lowering of glacial atmospheric CO₂ in response to changes in oceanic circulation and marine biogeochemistry, *Paleoceanography*, 22, PA4202, doi:10.1029/2006PA001380, 2007. 156
- Brovkin, V., Ganopolski, A., Archer, D., and Munhoven, G.: Glacial CO₂ cycle as a succession of key physical and biogeochemical processes, *Clim. Past*, 8, 251–264, doi:10.5194/cp-8-251-2012, 2012. 153
- Cakmur, R. V., Miller, R. L., Perlwitz, J., Geogdzhayev, I. V., Ginoux, P., Koch, D., Kohfeld, K. E., Tegen, I., and Zender, C. S.: Constraining the magnitude of the global dust cycle by minimizing the difference between a model and observations, *J. Geophys. Res.*, 111, D06207, doi:10.1029/2005JD005791, 2006. 152
- Calov, R., Ganopolski, A., Claussen, M., Petoukhov, V., and Greve, R.: Transient simulation of the last glacial inception, Part I: glacial inception as a bifurcation in the climate system, *Clim. Dynam.*, 24, 545–561, 2005. 156, 157
- Chin, M., Ginoux, P., and Kinne, S.: Tropospheric aerosol optical thickness from the GOCART model and comparisons with satellite and Sun photometer measurements, *J. Atmos. Sci.*, 59, 461–483, 2002. 152
- Christopher, S. A. and Jones, T.: Satellite-based assessment of cloud-free net radiative effect of dust aerosols over the Atlantic Ocean, *Geophys. Res. Lett.*, 34, L02810, doi:10.1029/2006GL027783, 2007. 164
- Claquin, T., Schulz, M., Balkanski, Y., and Boucher, O.: Uncertainties in assessing radiative forcing by mineral dust, *Tellus*, 50, 491–505, 1998. 155

**Sensitivity
simulations with dust
radiative forcing**

E. Bauer and
A. Ganopolski

[Title Page](#)[Abstract](#)[Introduction](#)[Conclusions](#)[References](#)[Tables](#)[Figures](#)[⏪](#)[⏩](#)[◀](#)[▶](#)[Back](#)[Close](#)[Full Screen / Esc](#)[Printer-friendly Version](#)[Interactive Discussion](#)

- Claquin, T., Roelandt, C., Kohfeld, K., Harrison, S., Tegen, I., Prentice, I. C., Balkanski, Y., Bergametti, G., Hansson, M., Mahowald, N., Rohde, H., and Schulz, M.: Radiative forcing of climate by ice-age atmospheric dust, *Clim. Dynam.*, 20, 193–202, 2003. 153, 154, 171
- 5 Claussen, M., Mysak, L., Weaver, A., Crucifix, M., Fichet, T., Loutre, M.-F., Weber, S., Alcamo, J., Alexeev, V., Berger, A., Calov, R., Ganopolski, A., Goosse, H., Lohmann, G., Lunkeit, F., Mokhov, I., Petoukhov, V., Stone, P., and Wang, Z.: Earth system models of intermediate complexity: closing the gap in the spectrum of climate system models, *Clim. Dynam.*, 18, 579–586, 2002. 156
- 10 Dentener, F., Kinne, S., Bond, T., Boucher, O., Cofala, J., Generoso, S., Ginoux, P., Gong, S., Hoelzemann, J. J., Ito, A., Marelli, L., Penner, J. E., Putaud, J.-P., Textor, C., Schulz, M., van der Werf, G. R., and Wilson, J.: Emissions of primary aerosol and precursor gases in the years 2000 and 1750 prescribed data-sets for AeroCom, *Atmos. Chem. Phys.*, 6, 4321–4344, doi:10.5194/acp-6-4321-2006, 2006. 151
- 15 Dubovik, O., Holben, B., Eck, T. F., Smirnov, A., Kaufman, Y. J., King, M. D., Tanre, D., and Slutsker, I.: Variability of absorption and optical properties of key aerosol types observed in worldwide locations, *J. Atmos. Sci.*, 59, 590–608, 2002. 155
- Ganopolski, A. and Calov, R.: The role of orbital forcing, carbon dioxide and regolith in 100 kyr glacial cycles, *Clim. Past*, 7, 1415–1425, doi:10.5194/cp-7-1415-2011, 2011. 156
- 20 Ganopolski, A. and Roche, D. M.: On the nature of lead–lag relationships during glacial–interglacial climate transitions, *Quaternary Sci. Rev.*, 28, 3361–3378, 2009. 156
- Ganopolski, A., Kubatzki, C., Claussen, M., Brovkin, V., and Petoukhov, V.: The influence of vegetation–atmosphere–ocean interaction on climate during the mid-Holocene, *Science*, 280, 1916–1919, 1998. 159
- 25 Ganopolski, A., Petoukhov, V., Rahmstorf, S., Brovkin, V., Claussen, M., Eliseev, A., and Kubatzki, C.: CLIMBER-2: a climate system model of intermediate complexity, Part II: model sensitivity, *Clim. Dynam.*, 17, 735–751, 2001. 156
- Ganopolski, A., Calov, R., and Claussen, M.: Simulation of the last glacial cycle with a coupled climate ice-sheet model of intermediate complexity, *Clim. Past*, 6, 229–244, doi:10.5194/cp-6-229-2010, 2010. 153, 156, 157
- 30 Ginoux, P., Horowitz, L. W., Ramaswamy, V., Geogdzhayev, I. V., Holben, B. N., Stenchikov, G., and Tie, X.: Evaluation of aerosol distribution and optical depth in the Geophysical Fluid Dynamics Laboratory coupled model CM2.1 for present climate, *J. Geophys. Res.*, 111, D22210, doi:10.1029/2005JD006707, 2006. 152

Sensitivity simulations with dust radiative forcing

E. Bauer and
A. Ganopolski

Title Page

Abstract

Introduction

Conclusions

References

Tables

Figures

⏪

⏩

◀

▶

Back

Close

Full Screen / Esc

Printer-friendly Version

Interactive Discussion

- Greve, R.: A continuum-mechanical formulation for shallow polythermal ice sheets, *Philos. T. Roy. Soc. Lond.*, 335, 921–974, 1997. 157
- Grini, A., Myhre, G., Zender, C. S., and Isaksen, I. S. A.: Model simulations of dust sources and transport in the global atmosphere: effects of soil erodibility and wind speed variability, *J. Geophys. Res.*, 110, D02205, doi:10.1029/2004JD005037, 2005. 152
- Haywood, J., Francis, P., Osborne, S., Glew, M., Loeb, N., Highwood, E., Tanre, D., Myhre, G., Formenti, P., and Hirst, E.: Radiative properties and direct radiative effect of Saharan dust measured by the C-130 aircraft during SHADE: 1. Solar spectrum, *J. Geophys. Res.*, 108, 8577, doi:10.1029/2002JD002687, 2003. 162
- Kinne, S., Schulz, M., Textor, C., Guibert, S., Balkanski, Y., Bauer, S. E., Bernsten, T., Berglen, T. F., Boucher, O., Chin, M., Collins, W., Dentener, F., Diehl, T., Easter, R., Feichter, J., Fillmore, D., Ghan, S., Ginoux, P., Gong, S., Grini, A., Hendricks, J., Herzog, M., Horowitz, L., Isaksen, I., Iversen, T., Kirkevåg, A., Kloster, S., Koch, D., Kristjansson, J. E., Krol, M., Lauer, A., Lamarque, J. F., Lesins, G., Liu, X., Lohmann, U., Montanaro, V., Myhre, G., Penner, J., Pitari, G., Reddy, S., Seland, O., Stier, P., Takemura, T., and Tie, X.: An AeroCom initial assessment – optical properties in aerosol component modules of global models, *Atmos. Chem. Phys.*, 6, 1815–1834, doi:10.5194/acp-6-1815-2006, 2006. 159, 161, 162, 166
- Kohfeld, K. E. and Harrison, S. P.: DIRTMAP: the geological record of dust, *Earth-Sci. Rev.*, 54, 81–114, 2001. 151, 159, 160
- Krinner, G., Boucher, O., and Balkanski, Y.: Ice-free glacial northern Asia due to dust deposition on snow, *Clim. Dynam.*, 27, 613–625, 2006. 153
- Lambert, F., Delmonte, B., Petit, J. R., Bigler, M., Kaufmann, P. R., Hutterli, M. A., Stocker, T. F., Ruth, U., Steffensen, J. P., and Maggi, V.: Dust-climate couplings over the past 800,000 yr from the EPICA Dome C ice core, *Nature*, 452, 616–619, 2008. 152
- Liao, H. and Seinfeld, J. H.: Radiative forcing by mineral dust aerosols: sensitivity to key variables, *J. Geophys. Res.*, 103, 31637–31645, 1998. 162, 163
- Liao, H., Seinfeld, J. H., Adams, P. J., and Mickley, L. J.: Global radiative forcing of coupled tropospheric ozone and aerosols in a unified general circulation model, *J. Geophys. Res.*, 109, D16207, doi:10.1029/2003JD004456, 2004. 152, 160
- Lunt, D. J. and Valdes, P. J.: The modern dust cycle: comparison of model results with observations and study of sensitivities, *J. Geophys. Res.*, 107, 4669, doi:10.1029/2002JD002316, 2002. 152

Sensitivity simulations with dust radiative forcing

E. Bauer and
A. Ganopolski

[Title Page](#)

[Abstract](#)

[Introduction](#)

[Conclusions](#)

[References](#)

[Tables](#)

[Figures](#)

[⏪](#)

[⏩](#)

[◀](#)

[▶](#)

[Back](#)

[Close](#)

[Full Screen / Esc](#)

[Printer-friendly Version](#)

[Interactive Discussion](#)



- Luo, C., Mahowald, N. M., and del Corral, J.: Sensitivity study of meteorological parameters on mineral aerosol mobilization, transport, and distribution, *J. Geophys. Res.*, 108, 4447, doi:10.1029/2003JD003483, 2003. 152, 160
- 5 Maher, B., Prospero, J., Mackie, D., Gaiero, D., Hesse, P., and Balkanski, Y.: Global connections between aeolian dust, climate and ocean biogeochemistry at the present day and at the last glacial maximum, *Earth-Sci. Rev.*, 99, 61–97, 2010. 151
- Mahowald, N., Kohfeld, K., Hansson, M., Balkanski, Y., Harrison, S. P., Prentice, I. C., Schulz, M., and Rodhe, H.: Dust sources and deposition during the last glacial maximum and current climate: a comparison of model results with paleodata from ice cores and marine sediments, *J. Geophys. Res.*, 104, 15895–15916, 1999. 153, 154, 157, 181
- 10 Mahowald, N. M., Muhs, D. R., Levis, S., Rasch, P. J., Yoshioka, M., Zender, C. S., and Luo, C.: Change in atmospheric mineral aerosols in response to climate: last glacial period, pre-industrial, modern, and doubled carbon dioxide climates, *J. Geophys. Res.*, 111, D10202, doi:10.1029/2005JD006653, 2006a. 152, 181
- 15 Mahowald, N. M., Yoshioka, M., Collins, W. D., Conley, A. J., Fillmore, D. W., and Coleman, D. B.: Climate response and radiative forcing from mineral aerosols during the last glacial maximum, pre-industrial, current and doubled-carbon dioxide climates, *Geophys. Res. Lett.*, 33, L20705, doi:10.1029/2006GL026126, 2006b. 152, 154, 161, 166, 170, 181
- 20 Martin, J. H.: Glacial–interglacial CO₂ change: the iron hypothesis, *Paleoceanography*, 5, 1–13, 1990. 153
- Miller, R. L., Cakmur, R. V., Perlwitz, J., Geogdzhayev, I. V., Ginoux, P., Koch, D., Kohfeld, K. E., Prigent, C., Ruedy, R., Schmidt, G. A., and Tegen, I.: Mineral dust aerosols in the NASA Goddard Institute for Space Sciences ModelE atmospheric general circulation model, *J. Geophys. Res.*, 111, D06208, doi:10.1029/2005JD005796, 2006. 152
- 25 Myhre, G. and Stordal, F.: Global sensitivity experiments of the radiative forcing due to mineral aerosols, *J. Geophys. Res.*, 106, 18193–18204, 2001. 155
- Myhre, G., Grini, A., Haywood, J. M., Stordal, F., Chatenet, B., Tanre, D., Sundet, K., and Isakson, I. S. A.: Modeling the radiative impact of mineral dust during the Saharan Dust Experiment (SHADE) campaign, *J. Geophys. Res.*, 108, 8579, doi:10.1029/2002JD002566, 2003. 152
- 30

Sensitivity simulations with dust radiative forcing

E. Bauer and
A. Ganopolski

[Title Page](#)[Abstract](#)[Introduction](#)[Conclusions](#)[References](#)[Tables](#)[Figures](#)[⏪](#)[⏩](#)[◀](#)[▶](#)[Back](#)[Close](#)[Full Screen / Esc](#)[Printer-friendly Version](#)[Interactive Discussion](#)

Osborne, S. R., Johnson, B. T., Haywood, J. M., Baran, A. J., Harrison, M. A. J., and McConnell, C. L.: Physical and optical properties of mineral dust aerosol during the Dust and Biomass-burning Experiment, *J. Geophys. Res.*, 113, D00C03, doi:10.1029/2007JD009551, 2008. 162

5 Otto, S., Bierwirth, E., Weinzierl, B., Kandler, K., Esselborn, M., Tesche, M., Schladitz, A., Wendisch, M., and Trautmann, T.: Solar radiative effects of a Saharan dust plume observed during SAMUM assuming spheroidal model particles, *Tellus B*, 61, 270–296, 2009. 155, 162, 163

Overpeck, J., Rind, D., Lacis, A., and Healy, R.: Possible role of dust-induced regional warming in abrupt climate change during the last glacial period, *Nature*, 384, 447–449, 1996. 155

10 Patadia, F., Gupta, P., and Christopher, S. A.: First observational estimates of global clear sky shortwave aerosol direct radiative effect over land, *Geophys. Res. Lett.*, 35, L04810, doi:10.1029/2007GL032314, 2008. 164

Patadia, F., Yang, E.-S., and Christopher, S. A.: Does dust change the clear sky top of atmosphere shortwave flux over high surface reflectance regions?, *Geophys. Res. Lett.*, 36, L15825, doi:10.1029/2009GL039092, 2009. 165

15 Petit, J. R., Jouzel, J., Raynaud, D., Barkov, N. I., Barnola, J. M., Basile, I., Bender, M., Chappellaz, J., Davis, M., Delaygue, G., Delmotte, M., Kotlyakov, V. M., Legrand, M., Lipenkov, V. Y., Lorius, C., Pepin, L., Ritz, C., Saltzman, E., and Stievenard, M.: Climate and atmospheric history of the past 420,000 yr from the Vostok ice core, Antarctica, *Nature*, 399, 429–436, 1999. 152, 157

20 Petoukhov, V., Ganopolski, A., Brovkin, V., Claussen, M., Eliseev, A., Kubatzki, C., and Rahmstorf, S.: CLIMBER-2: a climate system model of intermediate complexity, Part I: model description and performance for present climate, *Clim. Dynam.*, 16, 1–17, 2000. 156, 157, 163

25 Reddy, M. S., Boucher, O., Balkanski, Y., and Schulz, M.: Aerosol optical depths and direct radiative perturbations by species and source type, *Geophys. Res. Lett.*, 32, L12803, doi:10.1029/2004GL021743, 2005. 152, 155

30 Schneider von Deimling, T., Held, H., Ganopolski, A., and Rahmstorf, S.: Climate sensitivity estimated from ensemble simulations of glacial climate, *Clim. Dynam.*, 27, 149–163, 2006. 156

Sensitivity simulations with dust radiative forcing

E. Bauer and
A. Ganopolski

[Title Page](#)

[Abstract](#)

[Introduction](#)

[Conclusions](#)

[References](#)

[Tables](#)

[Figures](#)

[⏪](#)

[⏩](#)

[◀](#)

[▶](#)

[Back](#)

[Close](#)

[Full Screen / Esc](#)

[Printer-friendly Version](#)

[Interactive Discussion](#)

- Shettle, E. and Weinman, J.: The transfer of solar irradiance through inhomogeneous turbid atmospheres evaluated by Eddington's approximation, *J. Atmos. Sci.*, 27, 1048–1055, 1970. 163
- Sow, M., Alfaro, S. C., Rajot, J. L., and Marticorena, B.: Size resolved dust emission fluxes measured in Niger during 3 dust storms of the AMMA experiment, *Atmos. Chem. Phys.*, 9, 3881–3891, doi:10.5194/acp-9-3881-2009, 2009. 155
- Takemura, T., Egashira, M., Matsuzawa, K., Ichijo, H., O'ishi, R., and Abe-Ouchi, A.: A simulation of the global distribution and radiative forcing of soil dust aerosols at the Last Glacial Maximum, *Atmos. Chem. Phys.*, 9, 3061–3073, doi:10.5194/acp-9-3061-2009, 2009. 152, 153, 154, 167, 171, 181
- Tanaka, T. Y. and Chiba, M.: A numerical study of the contributions of dust source regions to the global dust budget, *Global Planet. Change*, 52, 88–104, 2006. 152
- Tegen, I. and Lacis, A. A.: Modeling of particle size distribution and its influence on the radiative properties of mineral dust aerosol, *J. Geophys. Res.*, 101, 19237–19244, 1996. 155
- Tegen, I., Lacis, A. A., and Fung, I.: The influence on climate forcing of mineral aerosols from disturbed soils, *Nature*, 380, 419–422, 1996. 155
- Tegen, I., Harrison, S. P., Kohfeld, K., and Prentice, I. C.: Impact of vegetation and preferential source areas on global dust aerosol: results from a model study, *J. Geophys. Res.*, 107, 4576, doi:10.1029/2001JD000963, 2002. 152
- Textor, C., Schulz, M., Guibert, S., Kinne, S., Balkanski, Y., Bauer, S., Berntsen, T., Berglen, T., Boucher, O., Chin, M., Dentener, F., Diehl, T., Easter, R., Feichter, H., Fillmore, D., Ghan, S., Ginoux, P., Gong, S., Grini, A., Hendricks, J., Horowitz, L., Huang, P., Isaksen, I., Iversen, I., Kloster, S., Koch, D., Kirkevåg, A., Kristjansson, J. E., Krol, M., Lauer, A., Lamarque, J. F., Liu, X., Montanaro, V., Myhre, G., Penner, J., Pitari, G., Reddy, S., Seland, Ø., Stier, P., Takemura, T., and Tie, X.: Analysis and quantification of the diversities of aerosol life cycles within AeroCom, *Atmos. Chem. Phys.*, 6, 1777–1813, doi:10.5194/acp-6-1777-2006, 2006. 151, 159
- Textor, C., Schulz, M., Guibert, S., Kinne, S., Balkanski, Y., Bauer, S., Berntsen, T., Berglen, T., Boucher, O., Chin, M., Dentener, F., Diehl, T., Feichter, J., Fillmore, D., Ginoux, P., Gong, S., Grini, A., Hendricks, J., Horowitz, L., Huang, P., Isaksen, I. S. A., Iversen, T., Kloster, S., Koch, D., Kirkevåg, A., Kristjansson, J. E., Krol, M., Lauer, A., Lamarque, J. F., Liu, X., Montanaro, V., Myhre, G., Penner, J. E., Pitari, G., Reddy, M. S., Seland, Ø., Stier, P., Takemura, T., and Tie, X.: The effect of harmonized emissions on aerosol properties in global models – an

**Sensitivity
simulations with dust
radiative forcing**

E. Bauer and
A. Ganopolski

[Title Page](#)[Abstract](#)[Introduction](#)[Conclusions](#)[References](#)[Tables](#)[Figures](#)[⏪](#)[⏩](#)[◀](#)[▶](#)[Back](#)[Close](#)[Full Screen / Esc](#)[Printer-friendly Version](#)[Interactive Discussion](#)

AeroCom experiment, *Atmos. Chem. Phys.*, 7, 4489–4501, doi:10.5194/acp-7-4489-2007, 2007. 151, 181

Waelbroeck, C., Paul, A., Kucera, M., Rosell-Melé, A., Weinelt, M., Schneider, R., Mix, A. C., Abelmann, A., Armand, L., Bard, E., Barker, S., Barrows, T. T., Benway, H., Cacho, I., Chen, M.-T., Cortijo, E., Crosta, X., de Vernal, A., Dokken, T., Duprat, J., Elderfield, H., Eynaud, F., Gersonde, R., Hayes, A., Henry, M., Hillaire-Marcel, C., Huang, C.-C., Jansen, E., Juggins, S., Kallel, N., Kiefer, T., Kienast, M., Labeyrie, L., Leclaire, H., Londeix, L., Mangin, S., Matthiessen, J., Marret, F., Meland, M., Morey, A. E., Mulitza, S., Pflaumann, U., Piasias, N. G., Radi, T., Rochon, A., Rohling, E. J., Saffi, L., Schäfer-Neth, C., Solignac, S., Spero, H., Tachikawa, K., and Turon, J.-L.: Constraints on the magnitude and patterns of ocean cooling at the Last Glacial Maximum, *Nat. Geosci.*, 2, 127–132, 2009. 166, 169

Warren, S. and Wiscombe, W.: A model for the spectral albedo of snow, II: snow containing atmospheric aerosols, *J. Atmos. Sci.*, 37, 2734–2745, 1980. 153

Watson, A. J., Bakker, D. C. E., Ridgwell, A. J., Boyd, P. W., and Law, C. S.: Effect of iron supply on Southern Ocean CO₂ uptake and implications for glacial atmospheric CO₂, *Nature*, 407, 730–733, 2000. 153

Werner, M., Tegen, I., Harrison, S. P., Kohfeld, K. E., Prentice, I. C., Balkanski, Y., Rohde, H., and Roelandt, C.: Seasonal and interannual variability of the mineral dust cycle under present and glacial climate conditions, *J. Geophys. Res.*, 107, 4744, doi:10.1029/2002JD002365, 2002. 152

Winckler, G., Anderson, R. F., Fleisher, M. Q., McGee, D., and Mahowald, N.: Covariant glacial–interglacial dust fluxes in the equatorial Pacific and Antarctica, *Science*, 320, 93–96, 2008. 152, 159

Yang, E.-S., Gupta, P., and Christopher, S. A.: Net radiative effect of dust aerosols from satellite measurements over Sahara, *Geophys. Res. Lett.*, 36, L18812, doi:10.1029/2009GL039801, 2009. 165

Sensitivity simulations with dust radiative forcing

E. Bauer and
A. Ganopolski

Table 2. Global dust deposition flux and dust load per area from three solutions of climate system model in off-line mode simulated at 21 ka (LGM) and 0 ka (PRE).

Solution	Deposition flux (Tgyr^{-1})		Dust load (mg m^{-2})	
	LGM	PRE	LGM	PRE
L0	3220	1710	83.3	43.9
L1	3220	1710	101.8	53.3
L2	3220	1710	63.5	33.7

[Title Page](#)
[Abstract](#)
[Introduction](#)
[Conclusions](#)
[References](#)
[Tables](#)
[Figures](#)
[Back](#)
[Close](#)
[Full Screen / Esc](#)
[Printer-friendly Version](#)
[Interactive Discussion](#)


Sensitivity simulations with dust radiative forcing

E. Bauer and
A. Ganopolski

Table 3. Global mean dust AOT and dust DRF at TOA from six simulations using solutions L1 and L2 and low, medium and high imaginary refractive index RI calculated at 21 ka (LGM) and 0 ka (PRE).

Experiment Solution	RI	Dust AOT		Dust DRF (Wm^{-2})	
		LGM	PRE	LGM	PRE
L1	0.0005	0.097	0.051	-0.92	-0.59
L2	0.0005	0.060	0.032	-0.65	-0.42
L1	0.0015	0.097	0.051	-0.66	-0.45
L2	0.0015	0.060	0.032	-0.50	-0.33
L1	0.0060	0.097	0.051	+0.04	-0.06
L2	0.0060	0.060	0.032	-0.06	-0.08

[Title Page](#)
[Abstract](#)
[Introduction](#)
[Conclusions](#)
[References](#)
[Tables](#)
[Figures](#)
[Back](#)
[Close](#)
[Full Screen / Esc](#)
[Printer-friendly Version](#)
[Interactive Discussion](#)


Sensitivity simulations with dust radiative forcing

E. Bauer and
A. Ganopolski

Table 4. Impact of dust DRF on global dust emission flux and dust AOT from six online simulations using solutions L1 and L2 and low, medium and high imaginary refractive index RI calculated at 21 ka (LGM) and 0 ka (PRE).

Experiment Solution	RI	Emission flux (Tgyr^{-1})		Dust AOT	
		LGM	PRE	LGM	PRE
L1	0.0005	3650	1730	0.116	0.050
L2	0.0005	3690	1740	0.070	0.032
L1	0.0015	3110	1600	0.096	0.047
L2	0.0015	3260	1640	0.061	0.031
L1	0.0060	2450	1380	0.072	0.040
L2	0.0060	2710	1480	0.051	0.028

[Title Page](#)
[Abstract](#)
[Introduction](#)
[Conclusions](#)
[References](#)
[Tables](#)
[Figures](#)
[⏪](#)
[⏩](#)
[◀](#)
[▶](#)
[Back](#)
[Close](#)
[Full Screen / Esc](#)
[Printer-friendly Version](#)
[Interactive Discussion](#)

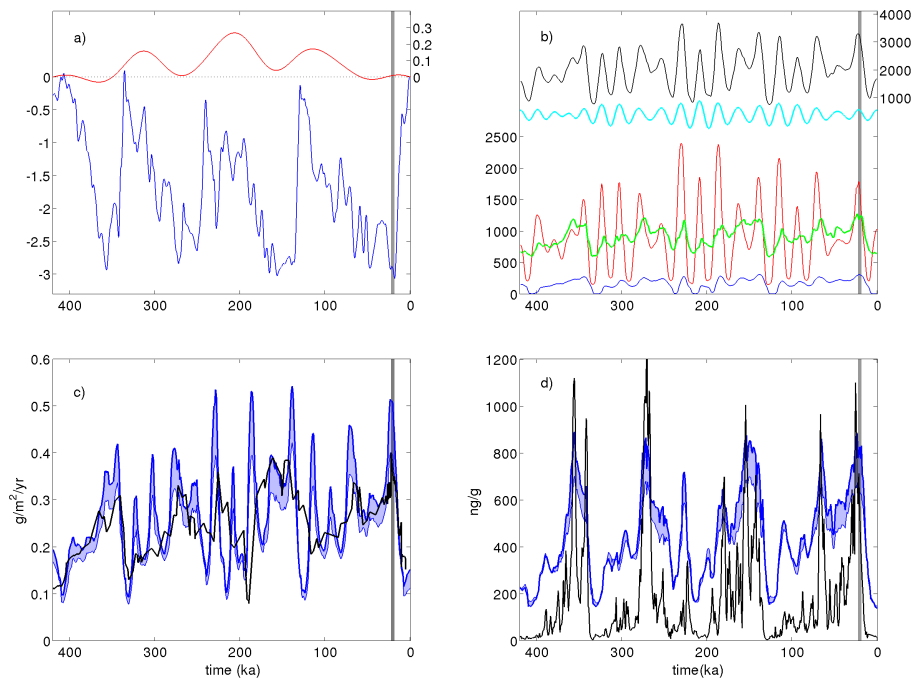

Sensitivity
simulations with dust
radiative forcingE. Bauer and
A. Ganopolski

Fig. 1. Forcing series for climate model **(a)** and simulated dust fluxes of emission **(b)** and deposition **(c, d)** for past 420 kyr. **(a)** Annual global mean radiative forcing relative to present day (W m^{-2}) from equivalent CO_2 concentration (blue line) and orbital-varying insolation (red line). **(b)** Global dust emission flux (Tgyr^{-1}) of total (black line) and partitions from deserts (red line), grass areas (green line) and exposed shelf areas (blue line), and climatic precession parameter in arbitrary units (cyan line). **(c)** Range of dust deposition flux (blue shaded) in $\text{mg m}^{-2} \text{yr}^{-1}$ for equatorial Pacific from solutions L1 (thick line) and L2 (thin line), respectively, compared to data (black line). **(d)** As in **(c)** but for dust concentration in ng g^{-1} for Antarctic ice. Vertical grey bars mark LGM period over 23–19 ka.

Sensitivity simulations with dust radiative forcing

E. Bauer and
A. Ganopolski

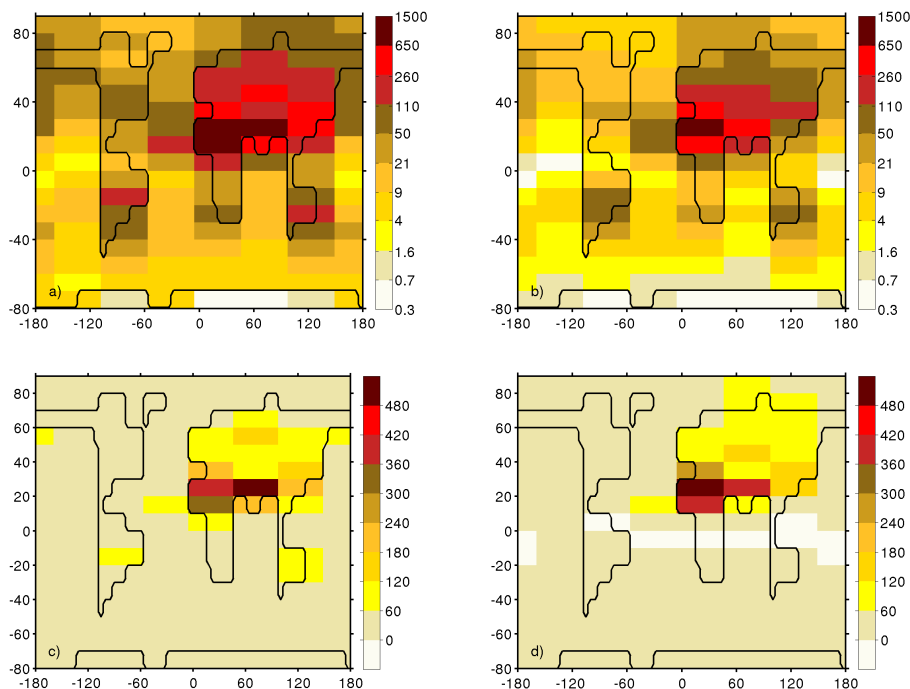
[Title Page](#)[Abstract](#)[Introduction](#)[Conclusions](#)[References](#)[Tables](#)[Figures](#)[Back](#)[Close](#)[Full Screen / Esc](#)[Printer-friendly Version](#)[Interactive Discussion](#)

Fig. 2. Geographic distributions of atmospheric dust load (mgm^{-2}) from solution L1 for 21 ka (a) and 0 ka (b) with logarithmic scale. Difference distributions of dust load shown with linear scale for 21 ka relative to 0 ka from solution L1 (c) and from solution L1 relative to solution L2 for 21 ka (d).

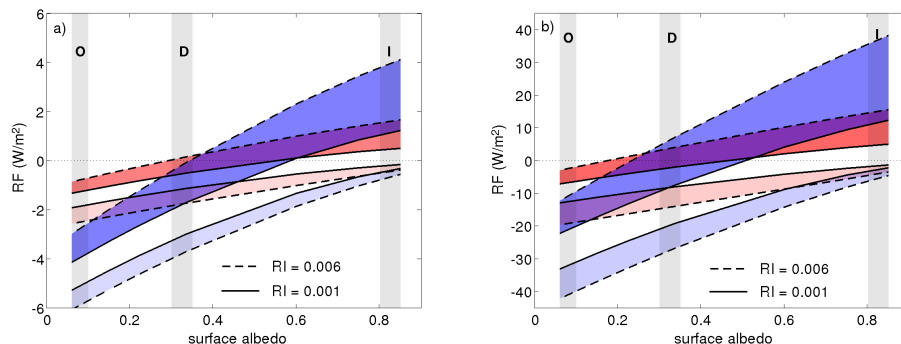
Sensitivity
simulations with dust
radiative forcingE. Bauer and
A. Ganopolski

Fig. 3. Annual global mean dust DRF as function of surface albedo simulated for dust load 100 mgm^{-2} (a) and 1000 mgm^{-2} (b). Boundaries of shaded areas obtained with $\text{RI} = 0.001$ and $\text{RI} = 0.006$ and radiative forcing at TOA (dark shading) and at surface (light shading) for clear sky conditions (blue shading) and for mean cloud fraction of 0.6 (red shading). Surface albedo typical for ocean, Sahara desert and ice/snow indicated by gray vertical bars marked with O, D and I, respectively.

Title Page

Abstract

Introduction

Conclusions

References

Tables

Figures

◀

▶

◀

▶

Back

Close

Full Screen / Esc

Printer-friendly Version

Interactive Discussion

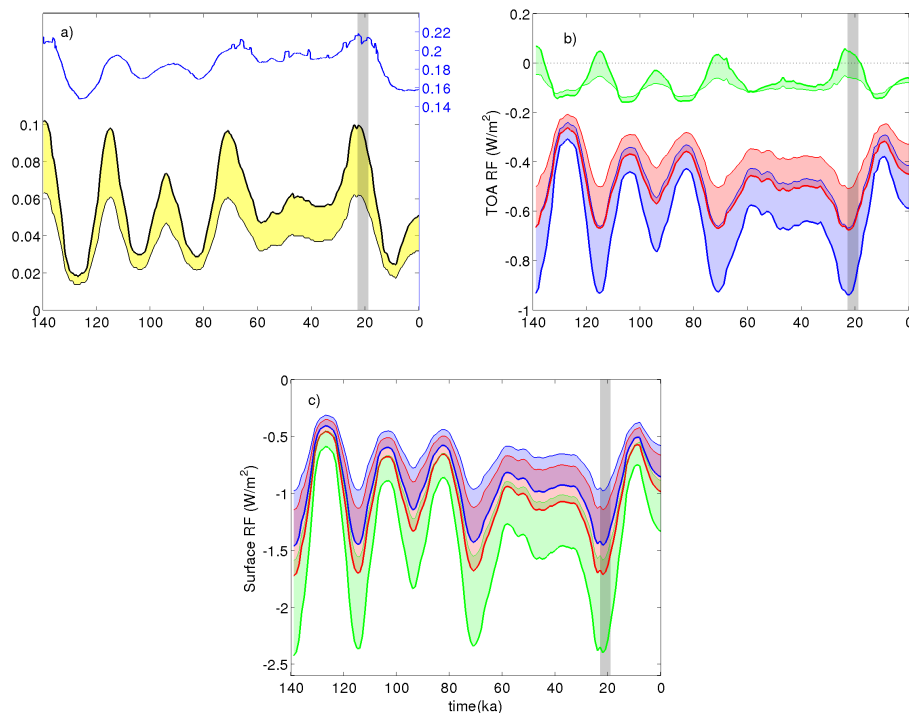
Sensitivity
simulations with dust
radiative forcingE. Bauer and
A. Ganopolski

Fig. 4. Annual global mean dust AOT **(a)** and dust DRF (W m^{-2}) at TOA **(b)** and at surface **(c)** for last 140 kyr. **(a)** Range of dust AOT (yellow shaded) from solutions L1 (thick line) and L2 (thin line), respectively, and surface albedo (blue line). **(b)** DRF at TOA for dust AOT from solutions L1 and L2 (line width as in **(a)**) using RI = 0.0005 (blue shaded), 0.0015 (red shaded) and 0.0060 (green shaded). **(c)** As in **(b)**, but for DRF at surface. Gray-shaded bars as in Fig. 1.

Title Page

Abstract

Introduction

Conclusions

References

Tables

Figures

◀

▶

◀

▶

Back

Close

Full Screen / Esc

Printer-friendly Version

Interactive Discussion

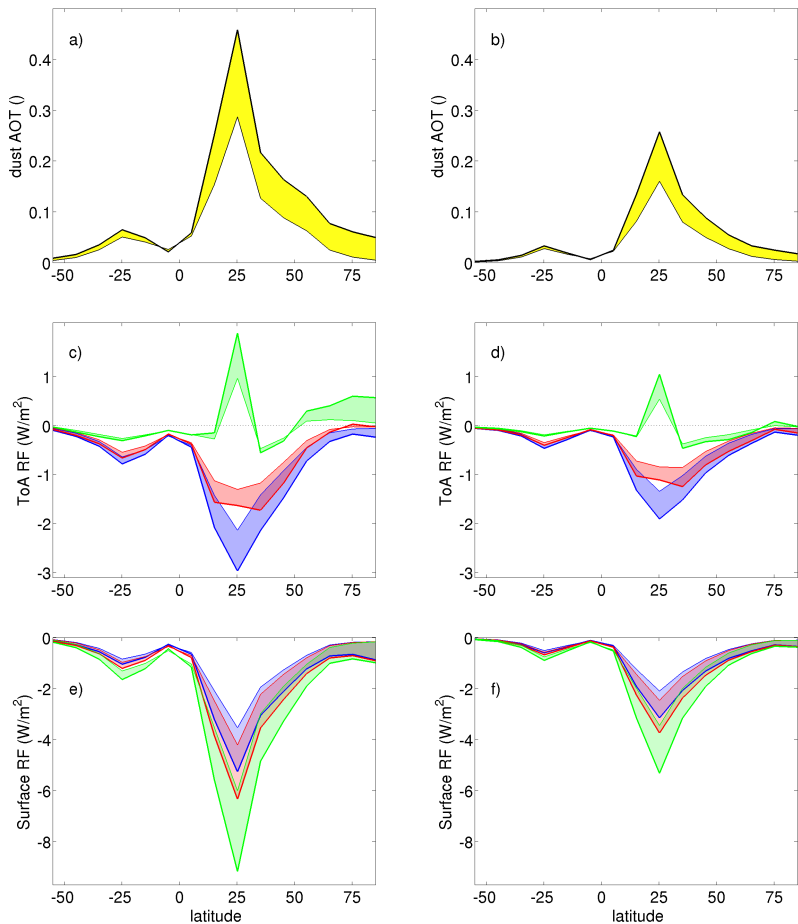


Fig. 5. Zonal means from off-line simulations for dust AOT (a, b), DRF (W m^{-2}) at TOA (c, d) and at surface (e, f) for 21 ka (a, c, e) and 0 ka (b, d, f). Color shading and line width as in Fig. 4.

Sensitivity simulations with dust radiative forcing

E. Bauer and
A. Ganopolski

Title Page

Abstract Introduction

Conclusions References

Tables Figures

⏪ ⏩

◀ ▶

Back Close

Full Screen / Esc

Printer-friendly Version

Interactive Discussion

Sensitivity simulations with dust radiative forcing

E. Bauer and
A. Ganopolski

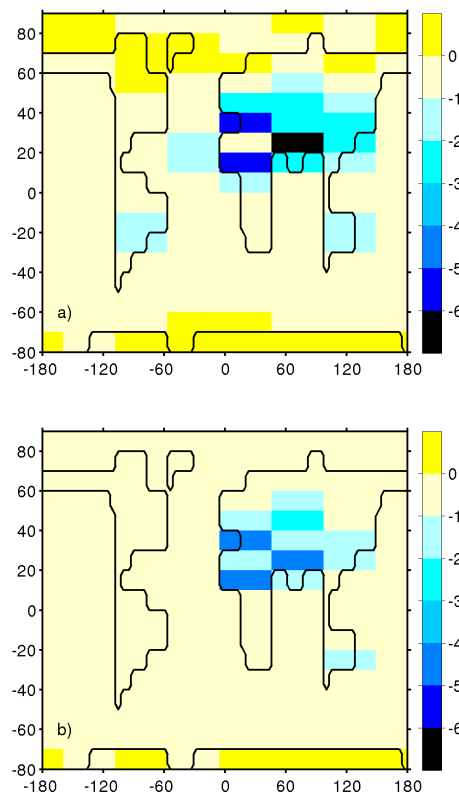
[Title Page](#)[Abstract](#)[Introduction](#)[Conclusions](#)[References](#)[Tables](#)[Figures](#)[Back](#)[Close](#)[Full Screen / Esc](#)[Printer-friendly Version](#)[Interactive Discussion](#)

Fig. 6. Geographic distributions of dust DRF at TOA (W m^{-2}) with dust load of solution L1 and $\text{RI} = 0.0015$ for 21 ka **(a)** and 0 ka **(b)**.

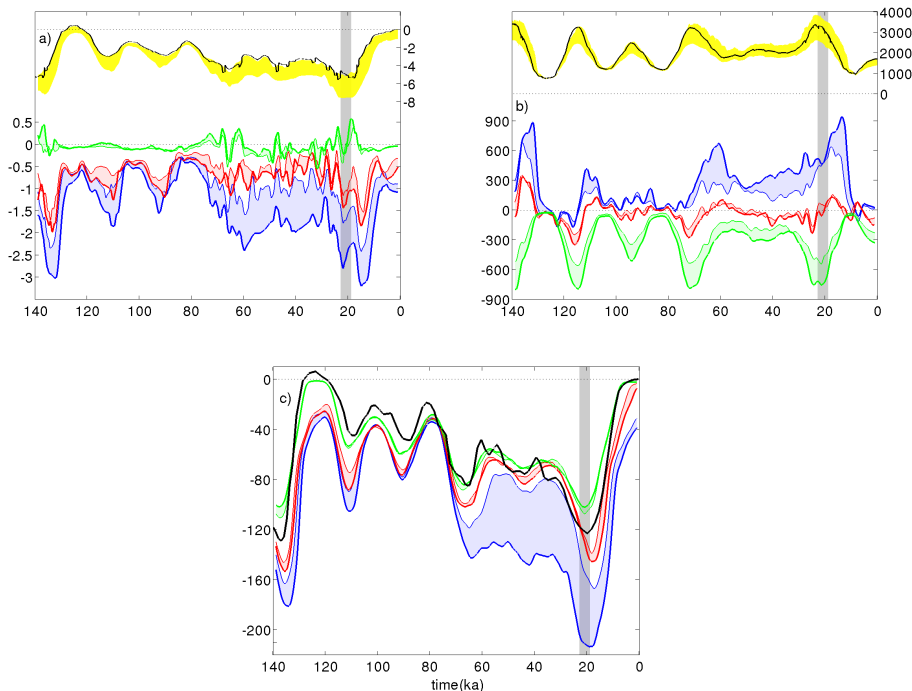


Fig. 7. Response to dust DRF from six online simulations for last 140 kyr. **(a)** SAT anomaly (K) relative to off-line SAT for RI = 0.0005, 0.0015 and 0.0060 (lower graphs with color shading and line width as in Fig. 4), and SAT difference of off-line simulation relative to present-day SAT (black line) compared to upper and lower SAT differences from online simulations with solution L1 and RI = 0.0005 and 0.0060 (yellow shaded). **(b)** Dust emission flux anomaly (T_{gyr}^{-1}) as in **(a)**, and total emission flux of off-line simulation (black line) and upper and lower emission fluxes from online simulations as in **(a)** (yellow shaded). **(c)** Sea level (m) from online simulations (color shading and line width as in **a**) compared to data (black line). Gray-shaded bars as in Fig. 1.

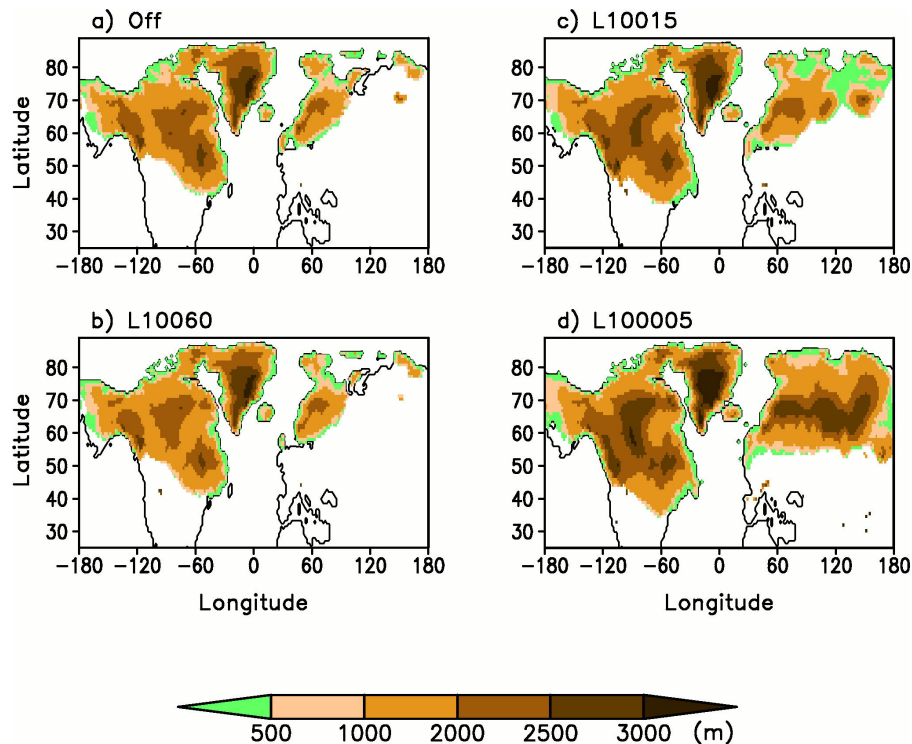
Sensitivity
simulations with dust
radiative forcingE. Bauer and
A. Ganopolski

Fig. 8. Simulated ice sheet extent and elevation (m) at the LGM in off-line experiment (a), and online experiments with solution L1 for $RI = 0.0060$ (b), $RI = 0.0015$ (c) and $RI = 0.00005$ (d).

[Title Page](#)[Abstract](#)[Introduction](#)[Conclusions](#)[References](#)[Tables](#)[Figures](#)[◀](#)[▶](#)[◀](#)[▶](#)[Back](#)[Close](#)[Full Screen / Esc](#)[Printer-friendly Version](#)[Interactive Discussion](#)

Sensitivity simulations with dust radiative forcing

E. Bauer and
A. Ganopolski

Title Page

Abstract

Introduction

Conclusions

References

Tables

Figures

⏪

⏩

◀

▶

Back

Close

Full Screen / Esc

Printer-friendly Version

Interactive Discussion

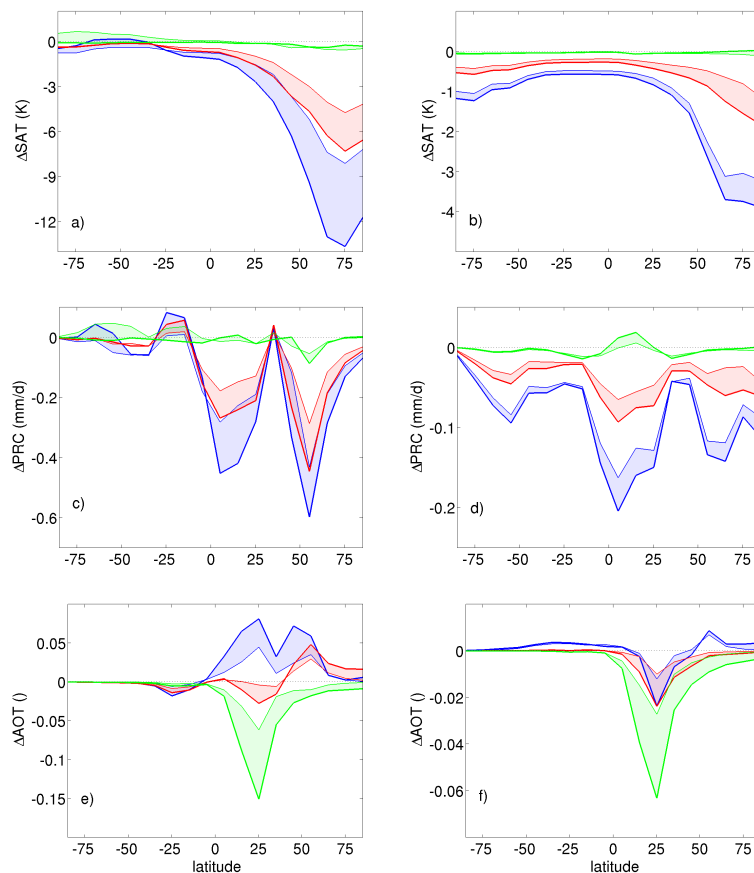


Fig. 9. Zonal means of response to dust DRF from six online simulations relative to off-line simulation for SAT in K (**a, b**), precipitation in mm d^{-1} (**c, d**) and dust AOT (**e, f**) for 21 kyr (**a, c, e**) and 0 ka (**b, d, f**). Color shading and line width as in Fig. 4.